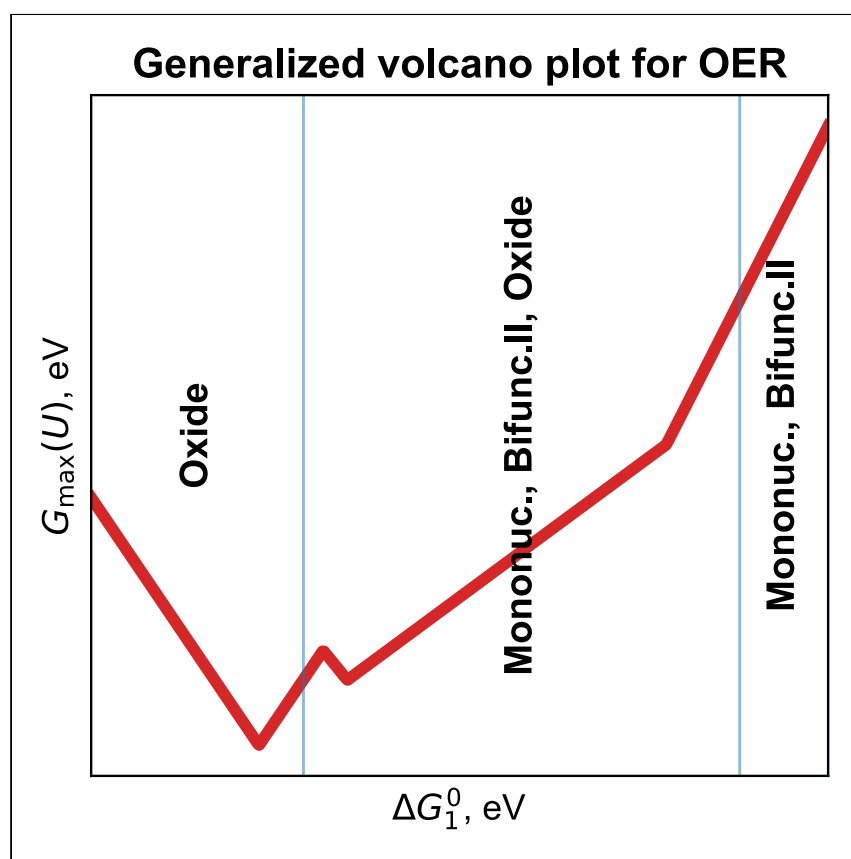


Article

Is the $*O$ vs. $*OH$ scaling relation intercept more relevant than the $*OOH$ vs. $*OH$ intercept to capture trends in the oxygen evolution reaction?



Oxygen evolution reaction (OER) hinders hydrogen production through electrocatalytic water splitting. The low activity of OER catalysts is linked to scaling relations (i.e., the linear dependence of free energies) between the reaction intermediates. In this article, we focus on the intercept of the largely overlooked scaling relation between the $*O$ and $*OH$ intermediates and demonstrate its importance to the OER volcano plot.

Maksim Sokolov, Kai S. Exner

kai.exner@uni-due.de

Highlights

$*O$ vs. $*OH$ scaling relation intercept impacts the shape of the volcano plot

Preferred reaction mechanism depends on the $*O$ vs. $*OH$ scaling relation intercept

Proposed generalized volcano plots capture experimental trends of RuO_2 and IrO_2



Sokolov & Exner, Chem Catalysis 4, 101039
July 18, 2024 © 2024 The Authors. Published by Elsevier Inc.

<https://doi.org/10.1016/j.cheecat.2024.101039>

Article

Is the *O vs. *OH scaling relation intercept more relevant than the *OOH vs. *OH intercept to capture trends in the oxygen evolution reaction?

Maksim Sokolov^{1,2} and Kai S. Exner^{1,2,3,4,5,*}

SUMMARY

The transition from fossil fuels to renewable energy sources is inevitable, and electrocatalytic water splitting to produce hydrogen is one of the core processes that must be further optimized. Regrettably, the anodic oxygen evolution reaction (OER) severely limits its efficiency. Theory explains the humble intrinsic activity of OER catalysts by scaling relations between reaction intermediates. While the scaling relation between the *OOH and *OH intermediates is well established, only the slope of the *O vs. *OH relation has an estimated numerical value, whereas the intercept of this scaling relation is frequently assumed to be zero. Herein, we demonstrate how deviations from this assumption cause changes in the shape of the volcano plot and the prevalent mechanisms at the apex of the volcano plot. Our derived volcano plots may enable further progress in the design of OER catalysts by shifting focus on the intercept of the *O vs. *OH scaling relation.

INTRODUCTION

Oxygen evolution reaction (OER) belongs to the most studied^{1–11} electrocatalytic processes due to its central importance as anodic counterreaction in proton exchange membrane electrolyzers for hydrogen production at the cathode of the device. In contrast to the kinetically facile hydrogen evolution reaction, large overpotentials of several hundred millivolts are experimentally observed to reach OER current densities of at least 10 mA/cm² for use in solar cell devices.¹²

The reason for the humble activity of OER catalysts is mainly attributed to its sluggish reaction kinetics, as four proton-electron pairs need to be transferred for the formation of a single oxygen molecule, $2\text{H}_2\text{O} \rightarrow \text{O}_2 + 4\text{H}^+ + 4\text{e}^-$, $U_{\text{OER}}^0 = 1.23 \text{ V}$ vs. reversible hydrogen electrode (RHE). In the last 15 years, electronic structure calculations in the density functional theory (DFT) approximation have been widely used to investigate the elementary steps of the OER over a variety of different materials, ranging from metals to metal oxides, sulfide-based materials, carbon-based materials, or high-entropy alloys.^{8,13–17} Most of these works rely on the assessment of the thermodynamics by determining the free energy changes, ΔG_i^0 ($i = 1, 2, 3, 4$), of the four proton-coupled electron transfer steps in the OER, which is facilitated by the application of the computational hydrogen electrode approach, as introduced by Nørskov and coworkers at the beginning of the 21st century.¹⁸ Independent of material class, the theoretical framework linked the low intrinsic activity of OER catalysts to a scaling relation^{19–23} in the reaction mechanism: it is commonly considered that the OER

THE BIGGER PICTURE

Green hydrogen, produced by electrocatalytic water splitting in electrolyzers using energy from renewable sources, is an environmentally friendly option for energy storage. To date, the anodic oxygen evolution reaction (OER) represents the main bottleneck for the large-scale implementation of electrolyzers due to the low intrinsic activity of OER catalysts. Theoretical studies have helped to gain mechanistic insight into the OER by identifying limiting factors at the atomistic level. There is a consensus in the literature that a scaling relationship between the *OOH and *OH intermediates in the mechanistic cycle limits the intrinsic activity of OER catalysts. On the other hand, the scaling relation between the *O and *OH intermediates has been largely ignored in identifying materials motifs for the OER. The present article demonstrates the importance of the *O vs. *OH scaling relation to understand activity trends and identify candidate materials using the concept of volcano plots.

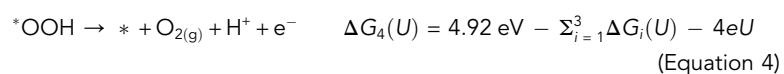
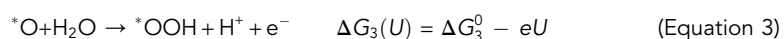
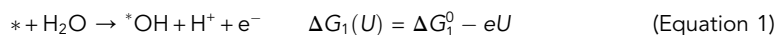
proceeds via the *OH, *O, and *OOH intermediates, and the free energy difference between the *OOH and *OH intermediates amounts to about 3.20 eV in a class of materials.¹³ This contrasts with the suggested optimum scaling relation intercept of a so-called ideal catalyst, which, based on the equilibrium potential of the OER, amounts to $2eU_{\text{OER}}^0 = 2.46$ eV.²⁴ Therefore, the deviation of 0.74 eV of the *OOH vs. *OH scaling relation from the thermodynamic ideal underpins that the OER is thermodynamically restrained,^{24,25} which may explain the slow reaction kinetics on the atomic scale. It should be noted that the concrete thermodynamic ideal intercept of the *OOH vs. *OH scaling relation is a matter of debate in the community as different viewpoints on the optimum intercept have been reported.^{26,27}

The *OOH vs. *OH scaling relation is commonly regarded as the main bottleneck for the development of highly active OER catalysts. To this end, the concept of scaling relations is often combined with the Sabatier principle²⁸ to construct volcano plots, which aid the understanding of activity trends of materials by means of heuristic activity descriptors.^{19,29–36} Besides the *OOH vs. *OH scaling relation in the OER, another scaling relation between the *O and *OH intermediates has been reported, which, however, is not as pronounced as the correlation between the *OOH and *OH adsorbates.^{8,20,37} So far, little attention has been paid to the *O vs. *OH scaling relation in previous studies.

In the present manuscript, we shed light on the importance of the *O vs. *OH scaling relation for the OER volcano plot as well as the design of highly active catalysts. In previous works, it has been assumed that the scaling coefficient of the *O vs. *OH scaling relation is equal to two without an intercept ($G_{*O} = 2G_{*OH}$). Using the dataset of Divanis et al. on metallic and semiconducting oxides from a decade of atomic scale simulations in the Rossmeisl and Nørskov groups,³⁷ we demonstrate that this correlation does not hold true in most cases. Rather, the *O vs. *OH scaling relation ($G_{*O} = \gamma_1 G_{*OH} + \xi_1$) is described by a scaling coefficient, γ_1 , and intercept, ξ_1 , which both deviate from two and zero, respectively. By applying an in-house data-driven strategy,^{38,39} we construct generalized volcano plots to assess the influence of the scaling coefficient and intercept of the *O vs. *OH scaling relation on activity trends in the OER. Notably, the intercept ξ_1 has a significant effect on the OER volcano curve, leading to a situation where two apexes, one global and one local, can be observed. Our revised OER volcano plots are able to comprehend the activity trends of IrO₂ and RuO₂, which are among the most active OER catalysts, for different pH values and motivate future studies by searching for correlations related to the *O and *OH adsorbates rather than the *OOH vs. *OH scaling relation.

Theoretical model

The elementary reaction steps of the OER include the subsequent formation of the *OH, *O, and *OOH intermediates,^{40,41} and the corresponding reaction mechanism is referred to as the mononuclear pathway, which is summarized in Equations 1, 2, 3, and 4.



¹University Duisburg-Essen, Faculty of Chemistry, Theoretical Inorganic Chemistry, Universitätsstraße 5, 45141 Essen, Germany

²Cluster of Excellence RESOLV, 44801 Bochum, Germany

³Center for Nanointegration (CENIDE) Duisburg-Essen, 47057 Duisburg, Germany

⁴X (formerly Twitter): @ExnerKai

⁵Lead contact

*Correspondence: kai.exner@uni-due.de

<https://doi.org/10.1016/j.cheecat.2024.101039>

In Equations 1, 2, 3, and 4, ΔG_i^0 ($i = 1, 2, 3, 4$) indicates the free energy change of the respective elementary reaction step at $U = 0$ V vs. RHE, and $\Delta G_i(U)$ refers to the free energy change at a given applied electrode potential U vs. RHE. The sum of the four free energy changes amounts to 4.92 eV = $4eU_{\text{OER}}^0$ at $U = 0$ V vs. RHE to meet the condition of electrochemical equilibrium, which is achieved by considering the concept of gas-phase error corrections⁴² in the analysis.

Based on the free energy changes of Equations 1–4, we can specify the free energies of the reaction intermediates *OH, *O, and *OOH as follows (cf. Equations 5, 6, 7, and 8):

$$G_*(U) = 0 \quad (\text{Equation 5})$$

$$G^{*\text{OH}}(U) = \Delta G_1(U) = \Delta G_1^0 - eU \quad (\text{Equation 6})$$

$$G^{*\text{O}}(U) = \Delta G_1(U) + \Delta G_2(U) = \Delta G_1^0 + \Delta G_2^0 - 2eU \quad (\text{Equation 7})$$

$$G^{*\text{OOH}}(U) = \Delta G_1(U) + \Delta G_2(U) + \Delta G_3(U) = \Delta G_1^0 + \Delta G_2^0 + \Delta G_3^0 - 3eU \quad (\text{Equation 8})$$

$$G^{*+\text{O}_2(\text{g})}(U) = \sum_{i=1}^4 \Delta G_i(U) = 4.92 \text{ eV} - 4eU \quad (\text{Equation 9})$$

It is noteworthy that the values of free energies are not entirely independent from each other since they are connected through the so-called scaling relations.^{13,43,44}

For the OER, two major scaling relations have been reported. One scaling relation refers to the *O and *OH intermediates (cf. Equation 10), whereas the other scaling relationship is encountered between the *OOH and *OH adsorbates (cf. Equation 11):

$$G^{*\text{O}} = \gamma_1 G^{*\text{OH}} + \xi_1 \quad (\text{Equation 10})$$

$$G^{*\text{OOH}} = \gamma_2 G^{*\text{OH}} + \xi_2 \quad (\text{Equation 11})$$

In Equations 10 and 11, γ_1 or γ_2 are dimensionless slope coefficients, and ξ_1 or ξ_2 denote the intercept of the respective scaling relation. Please note that in the literature, scaling relations are often expressed in terms of energies, E , rather than free energies, G , since the impact of zero-point energy and entropic corrections on the free energy can be considered negligible in a homologous series of materials.¹⁸

By rewriting Equations 10 and 11, we relate the above scaling relations to the respective free energy changes, ΔG_i^0 ($i = 1, 2, 3$), of the mononuclear mechanism (cf. Equations 12 and 13):

$$\Delta G_2^0 = \gamma_1' \Delta G_1^0 + \xi_1' \quad (\text{Equation 12})$$

$$\Delta G_3^0 = \gamma_2' \Delta G_2^0 + \xi_2' = \gamma_1' \gamma_2' \Delta G_1^0 + \gamma_2' \xi_1' + \xi_2' \quad (\text{Equation 13})$$

Similar to Equations 10 and 11, γ_1' or γ_2' and ξ_1' or ξ_2' denote the dimensionless slope coefficients and intercepts, respectively. Note that the relationships between the coefficients of Equations 10 and 12 are given by $\gamma_1' = \gamma_1 - 1$ and $\xi_1' = \xi_1$. To determine the values of γ_2' and ξ_2' , we utilize the fact that the slope coefficient and intercept of the scaling relation in Equation 11 are well-accepted to be $\gamma_2 = 1$ and $\xi_2 = 3.2$ eV, respectively.^{13,37–41,45–56}

Consequently, we arrive at $\gamma_2' = -1$ and $\xi_2' = \xi_2 = 3.2$ eV. We further refer to these values in the results section. For a detailed discussion on the slope coefficients and intercept, we refer to the literature.^{13,57}

The numerical values used in previous works that focus on the construction of volcano plots and the understanding of activity trends relating to the scaling relation of Equation 12 are $\gamma_1 = 2$, $\gamma'_1 = 1$, and $\xi_1 = \xi'_1 = 0$.^{31,58–60} However, there are studies that have reported values of the intercept of the *O vs. *OH scaling relation, $\xi_1 = \xi'_1$, that deviate from zero.^{25,61} This finding motivates to inspect the impact of the *O vs. *OH scaling on the OER activity volcano plot in the present contribution.

While initially it was assumed that the trends of OER catalysts can be described by volcano analyses based on the mononuclear mechanism only,^{13,41} there is clear evidence in the literature that materials in a homologous series do not necessarily comply with the same mechanism. Following a recent volcano-approach study by one of the authors,³⁹ in the present study, we factor a plethora of different pathways, namely the bifunctional I,⁴⁵ bifunctional II,^{45–47} binuclear,^{48,49} and oxide⁵⁰ mechanisms, into our data-driven assessment of the OER volcano plot. These mechanistic descriptions are summarized in section S1 of the [supplemental information](#), and they are subjected to a dedicated thermodynamic analysis discussed in section S2 of the [supplemental information](#). Based on the derived free energy expressions, we determine the electrocatalytic activity in the approximation of the descriptor $G_{\max}(U)$,^{51,52} which is based on the free energy span model.⁶² The choice of this activity measure is corroborated by the fact that it is a more accurate descriptor than the conventionally applied thermodynamic overpotential, η_{TD} ,⁶³ due to the imitation of overpotential and kinetic effects in the evaluation of adsorption free energies to assess activity trends. Note that we assess $G_{\max}(U)$ at an applied electrode potential of $U = 1.60$ V vs. RHE. This electrode potential can be related to typical experimental reaction conditions to achieve a current density on the order of at least 10 mA/cm².

In section S3 of the [supplemental information](#), we summarize the application of $G_{\max}(U)$ to all OER mechanisms in question. Activity predictions by $G_{\max}(U)$ and variation of the ξ'_1 intercept culminate in one-dimensional volcano plots with ΔG_1^0 as a variable and ξ'_1 as a parameter (cf. [Figure S1](#) in section 4 of the [supplemental information](#)). Further details of the volcano plot construction are provided in section S4 of the [supplemental information](#), where we discuss the choice of parameters of our data-driven analysis. Additional information on our modeling approach can also be found in the literature,³⁸ where our in-house methodology has been dedicatedly explained. The main idea of our investigation is to vary ΔG_1^0 and to track changes in the preferred reaction mechanism(s) in the OER volcano plot by using “inexact matching” of the descriptor $G_{\max}(U)$; this technique is further explained in section S4 of the [supplemental information](#). While we emphasize that our group has recently published several papers on the impact of various reaction mechanisms on the volcano plot^{39,64–67} for a variety of electrocatalytic processes including the OER, the present study breaks new ground by discussing the impact of the *O vs. *OH scaling relation intercept (cf. [Equation 12](#)) on the volcano plot. This appears to be an important factor that, hitherto, has been largely overlooked in the discussion of volcano curves, whereas the scaling relation intercept between the *OOH vs. *OH adsorbates (cf. [Equation 13](#)) has been extensively investigated in previous works.^{13,25,44,68}

RESULTS

We start our analysis by replicating the reference data by Divanis et al.³⁷ (cf. [Figure 1](#)). This dataset comprises the free energy changes, ΔG_i^0 ($i = 1, 2, 3, 4$), of the mononuclear mechanism (cf. [Equations 1, 2, 3, and 4](#)) for a variety of metal oxides, including pristine and doped materials. The choice of this dataset is 2-fold: first, metal oxides are among the most active OER catalysts by referring to IrO₂ and RuO₂.⁶⁹ Second, even if the calculated adsorption free energies depend on the chosen computational

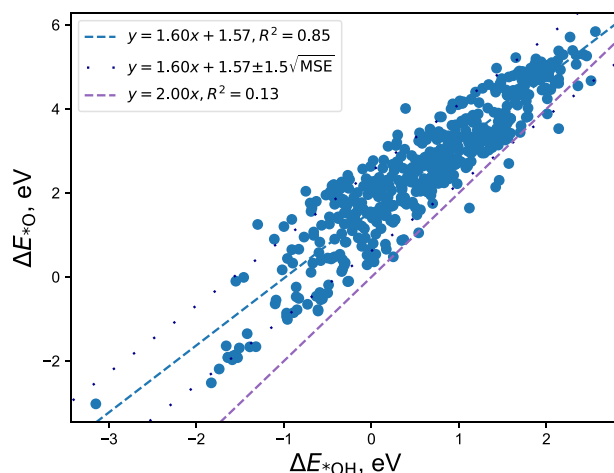


Figure 1. Data for the scaling relation between the adsorption energies of the *O and *OH intermediates

Blue dashed line: linear regression result. Purple dashed line: conventional scaling relation considered for the construction of volcano plots. Dark blue dotted line: linear regression of the best-fit line shifted up or down by 1.5 times the square root of the mean squared error (MSE), $\sqrt{\text{MSE}} = 0.63$ eV. Data taken from the work by Divanis et al.³⁷

parameters with respect to the exchange correlation functional, the scaling relations based on the free energy changes ΔG_i^0 ($i = 1, 2, 3, 4$) are largely invariant to the computational settings, as discussed in a recent analysis of this dataset to comprehend the OER at the atomic level.⁷⁰

Please note that in Divanis' work, adsorption energies rather than adsorption free energies are reported, thus relying on the tacit assumption that the contribution of zero-point energy and entropic corrections to the free energy changes is negligible in a homologous series of materials. Figure 1 indicates that the best-fit line of the *O vs. *OH scaling relation reveals $\gamma_1 = 1.60$ ($\gamma_1' = 0.60$) and $\xi_1 = 1.57$ eV ($\xi_1' = 1.57$ eV) (cf. Equations 10, 11, 12, and 13); these values differ significantly from the commonly assumed values of $\gamma_1 = 2.00$ ($\gamma_1' = 1.00$) and $\xi_1 = 0.00$ eV ($\xi_1' = 0.00$ eV).^{31,58–60} This surprising finding motivated us to further inspect the impact of a slope smaller than 2 and an intercept different than 0 on the OER activity volcano plot.

In a recent communication, Exner constructed OER volcano plots based on the outlined modeling scheme. The author arrived at the conclusion that the OER activity volcano is governed by different mechanistic descriptions in dependence on the descriptor ΔG_1^0 , and the preferred pathway can change upon increasing overpotential. In Exner's work, the following parameters were used for the *O vs. *OH scaling relation: $\gamma_1' = 2.00$ and $\xi_1' = 0.00$ eV. A side remark is needed for the choice of $\gamma_1' = 2.00$: this value refers to the notion that the *O intermediate might bind via a double bond, whereas the *OH adsorbate binds via a single bond to the catalyst surface. While it would be better to apply $\gamma_1 = 2.00$ rather than $\gamma_1' = 2.00$ for this train of thought, the main conclusions of Exner's work relating to a switch of the reaction mechanism with increasing overpotential remain unchanged, independent of the usage of $\gamma_1' = 2.00$ or $\gamma_1' = 1.00$ ($\gamma_1 = 2.00$) in the generalized analysis of activity volcano plots.³⁹

The above-discussed finding underpins that a change in the slope of the *O vs. *OH scaling relation is relatively insignificant to the OER volcano plot, and we come back

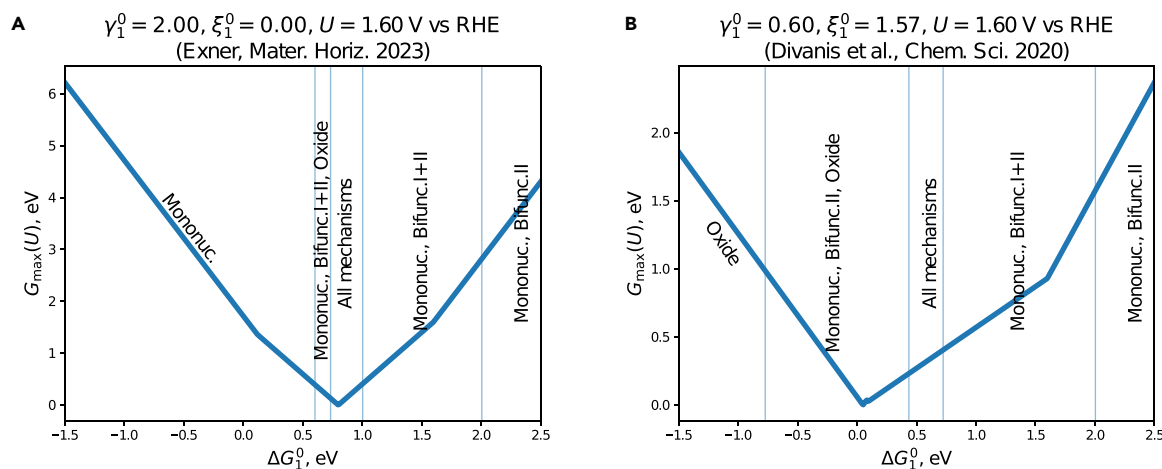


Figure 2. Mechanistic volcano plots with different *O vs. *OH scaling relation parameters

(A) Mechanistic volcano plot by using γ_1^0 and ξ_1^0 of Exner's recent work.³⁹

(B) Mechanistic volcano plot by using γ_1^0 and ξ_1^0 of Divanis' work (cf. Figure 1).³⁷ Please note that the plot in (A) is slightly different from the original in Exner³⁹ due to the inexact matching applied in our methodology (cf. section S4 of the supplemental information).

to this statement at the end of this section again. However, a different situation is encountered for the intercept of the scaling relation between the *O and *OH intermediates. Figure 2 compares the volcano plot of Exner's recent contribution to the volcano plot based on the dataset of Divanis et al.³⁷ (cf. scaling relation of Figure 1). In the supplemental information, we have also provided volcano plots for the intercept of the *O vs. *OH scaling relation obtained by the dataset of Divanis et al. including the consideration of error bars using the square root of the mean squared error (cf. Figures S2–S10 in section S5).

It is directly visible that the apex of the volcano plot shifts to the left (stronger *OH binding) by about 0.8 eV if the intercept of the *O vs. *OH scaling relation increases from 0 eV to 1.6 eV. This significant displacement of the volcano apex is unexpected but clearly substantiates that, hitherto, the intercept of the *O vs. *OH scaling relation has been largely overlooked for volcano analyses. Also, the prevalent mechanism on the left leg of the volcano plot (strong *OH binding) switches from the mononuclear to the oxide description, indicating that a variation in the intercept can alter the energetically preferred pathway in the OER. Finally, it is qualitatively visible that the legs of the two volcano plots largely differ relating to the activity descriptor $G_{\max}(U)$: for an intercept of 0 eV, the decrease in the electrocatalytic activity is much more pronounced than for the intercept of 1.6 eV. This observation can be related to the different slopes of the two plots since $\gamma_1^0 = 2.00$ is accompanied with a much steeper volcano slope⁷¹ than $\gamma_1^0 = 0.60$.

Due to the unexpected influence of the *O vs. *OH scaling relation on the OER activity volcano, we generalize our study by monitoring the influence of a varying intercept of the *O and *OH intermediates on the volcano curve, which is further discussed below. Here, we consider $\xi_1^0 \in [-1.50; 2.50]$ eV with a step size of 0.50 eV in the analysis. A detailed overview of the respective volcano curves is provided in section S5 of the supplemental information (cf. Figures S2–S10). In the following, we focus on $\xi_1^0 \in [1.00; 2.50]$ eV as this value range captures the most important effects. The discussed value range for ξ_1^0 is also corroborated by a recent study of Man and Tranca based on the same dataset, reporting values of $0.78 \text{ eV} \leq \xi_1^0 \leq 2.78 \text{ eV}$ by

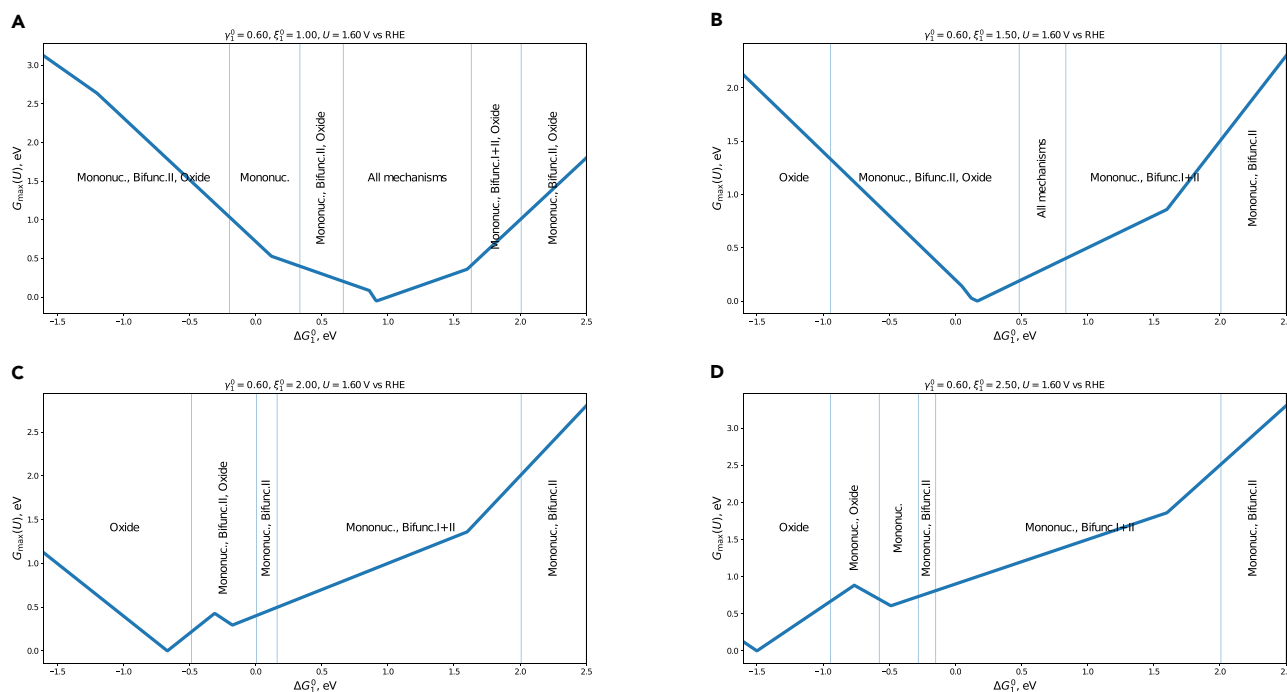


Figure 3. Mechanistic OER volcano plots using $\gamma_1' = 0.60$ and variable values for ξ_1'

- (A) $\xi_1' = 1.00$ eV.
 (B) $\xi_1' = 1.50$ eV.
 (C) $\xi_1' = 2.00$ eV.
 (D) $\xi_1' = 2.50$ eV.

The value for γ_1' is taken from Divanis et al.³⁷ For a more detailed overview, we refer the reader to Figures S2–S10 in section S5 of the supplemental information.

clustering the *O vs. *OH scaling relation intercept into intervals based on the evaluation of the thermodynamic overpotential.⁷⁰

OER volcano curves in dependence of ξ_1' are depicted in Figure 3. We distinguish two key aspects of a changing intercept for the *O vs. *OH scaling relation, namely the mechanistic profile and the shape of the volcano. Our results illustrate that for $\xi_1' \geq 2.00$ eV, the binuclear mechanism is not observed in the OER volcano plot anymore. This finding contrasts with Figure 2A or smaller intercepts ($\xi_1' < 2.00$ eV), indicating that in these cases the binuclear description is mainly observed close to or at the volcano apex under typical OER conditions. Therefore, it can be concluded that a non-zero intercept may cause that certain mechanistic descriptions can be largely excluded *a priori* by means of generalized volcano analyses; this information is significant to materials modeling of OER catalysts by means of DFT calculations as it reduces computational costs.

Besides, the appearance of the oxide mechanism in the volcano plot strongly depends on the intercept of the *O vs. *OH scaling relation. While this pathway is observed at the weak-binding volcano leg for an intercept of $\xi_1' = 1.00$ eV, for larger values of this intercept, the oxide description becomes preferred at the opposite volcano leg corresponding to strong *OH binding.

While the mononuclear mechanism is still the most commonly applied mechanistic description in DFT studies, the volcano curves of Figure 3 underpin its relevance to the OER modeling as this mechanism is part of the volcano plot in almost all

cases, except in the case of strong *OH binding for $\xi'_1 > 1.00$ eV. Nonetheless, the consideration of the mononuclear description only for the approximation of the electrocatalytic activity can lead to wrong conclusions since in most intervals of the descriptor ΔG_1^0 , the mononuclear pathway competes with another reaction mechanism.⁷²

It is noteworthy that both the bifunctional I and II mechanisms are almost as prevalent as the mononuclear description in the volcano plots with various intercepts. It is evident that in the case of a larger intercept, the bifunctional I pathway already appears at stronger *OH binding ($\Delta G_1^0 \approx 0.6$ eV at $\xi'_1 = 1.00$ eV vs. $\Delta G_1^0 \approx -0.1$ eV at $\xi'_1 = 2.50$ eV). On the other hand, the bifunctional I mechanism is not operative for weak *OH binding of $\Delta G_1^0 > 2.0$ eV, regardless of the value of ξ'_1 . Relating to the bifunctional II description, it is important to indicate that the appearance of this mechanistic pathway in the volcano plot is shifted to weaker *OH binding with increasing intercept ($\Delta G_1^0 \approx -0.9$ eV at $\xi'_1 = 1.50$ eV vs. $\Delta G_1^0 \approx -0.3$ eV at $\xi'_1 = 2.50$ eV). Overall, there are more mechanistic changes for strong *OH binding ($\Delta G_1^0 < 0.0$ eV), whereas the range of weak *OH binding ($\Delta G_1^0 > 0.5$ eV) is not largely affected by a varying intercept.

In the following, we discuss the shape of the OER volcano. Figure 3 illustrates that with increasing intercept, the volcano apex is strongly shifted to the left, indicating a preference for strong *OH binding. The same trend is observed even if we consider only the mononuclear mechanism and use η_{TD} as the activity descriptor, as discussed in section S6 of the supplemental information (cf. Figure S11). Notably, for $\xi'_1 = 2.00$ eV and $\xi'_1 = 2.50$ eV, a second minimum arises in the volcano plot at a slightly larger ΔG_1^0 value compared to the global minimum (in the case of $\xi'_1 = 2.00$: $\Delta G_1^0 = -0.67$ eV and $\Delta G_1^0 = -0.17$ eV for the global and the local minima, respectively). The appearance of this local minimum is accompanied by a switch in the preferred reaction mechanism at the global volcano apex. While for $\xi'_1 < 2.00$ eV the mechanistic diversity is clearly pronounced since at least three or even all mechanisms govern the volcano top, only the oxide mechanism is observed at the global volcano apex for $\xi'_1 = 2.00$ eV and $\xi'_1 = 2.50$ eV.

Additionally, we examine the slope of the *O vs. *OH scaling relation by means of sensitivity analyses. In this context, we fix the value of the intercept by using $\xi'_1 = 1.57$ eV and vary the slope γ'_1 in the range of 0.22–1.00 (γ_1 from 1.22 to 2.00); the former is the lowest value from the study of Divanis et al.,³⁷ and the latter corresponds to the conventional value in previous studies. Our results are summarized in Figure 4 and demonstrate that an altered slope has a minor quantitative but not a qualitative effect on the OER activity volcano, in agreement with Exner's recent study.³³ More precisely, the legs of the volcano become steeper as the slope γ'_1 increases, indicating that the electrocatalytic activity is reduced more rapidly when moving away from the volcano top. Even if there are certain shifts in the ΔG_1^0 ranges for the windows of prevalent mechanisms, the overall profile remains unchanged. Most importantly, we can clearly see that the volcano apex and the prevalent mechanisms at the apex do not change, which contrasts with the varying intercept (cf. Figure 3). Therefore, we can confidently render the conclusion that the intercept, ξ'_1 , of the *O vs. *OH scaling relation is of higher relevance to the OER volcano plot than the slope, γ'_1 , of this scaling relation. While the concrete range of ξ'_1 for different classes of OER materials is yet to be determined, we outline a new train of thought in the discussion section of our manuscript of how to make use of the intercept ξ'_1 for materials discovery and catalyst optimization.

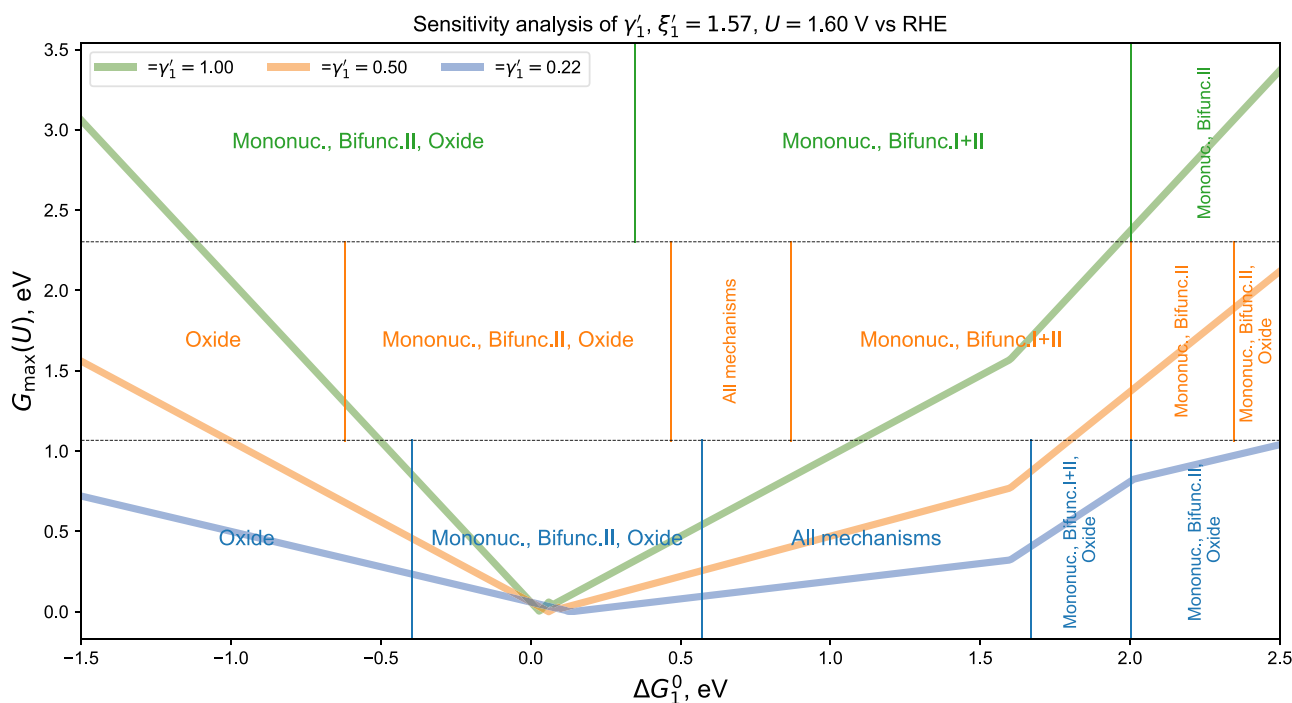


Figure 4. Mechanistic OER volcano plot to demonstrate its sensitivity to three values of γ_1 , namely $\gamma_1 = 0.22$ (blue), $\gamma_1 = 0.50$ (orange), and $\gamma_1 = 1.00$ (green).

So far, we have discussed the OER volcano plot in a generalized fashion by inspecting the impact of the *O vs. *OH scaling relation on the preferred reaction mechanism and shape of the volcano. In the next step, we benchmark the derived volcano plots with experimental data. Due to the fact that the dataset of Divanis et al.³⁷ focuses on metal oxides, we discuss activity trends for single-crystalline IrO₂(110) and RuO₂(110) electrodes. It is noteworthy that Kuo et al. have determined the ΔG_i^0 ($i = 1, 2$) values of the mononuclear mechanism (cf. Equations 1, 2, 3, and 4) for both model electrodes at different pH values based on cyclic voltammetry measurements.^{53,54} These values are summarized in Table S1 of the supplemental information, and Table S2 compiles the activity trends of IrO₂(110) and RuO₂(110) in the OER for different electrolyte solutions (cf. section S7 of the supplemental information).

Based on the experimental data, we determine the slope γ_1 and scaling relation intercept ξ_1^0 of the *O vs. *OH scaling relation for both materials (cf. Figure 5A), which are distinct for IrO₂(110) and RuO₂(110). Using these two scaling relations, we compile volcano plots for IrO₂(110) and RuO₂(110) at $U = 1.60$ V vs. RHE (cf. Figure 5B). It is evident that the apex of the volcano plot for RuO₂(110) is below that of IrO₂(110), indicating that RuO₂(110) should be in general more active than IrO₂(110) in the OER, which is consistent with experimental data^{69,73} from different laboratories. When discussing the activity of these materials in acid (pH = 1) or base (pH = 12.9) by including the respective ΔG_1^0 values (cf. Table S1) as data points in the volcano plot, we conclude that RuO₂(110) is more active in acid than in base, which is in line with the experimental results of Kuo and coworkers (cf. Table S2). In case of IrO₂(110), we observe that the electrocatalytic activity in acid and base is almost identical, which agrees reasonably well with the reported slightly higher electrocatalytic activity of IrO₂(110) under acidic conditions (cf. Table S2). Finally, it is also

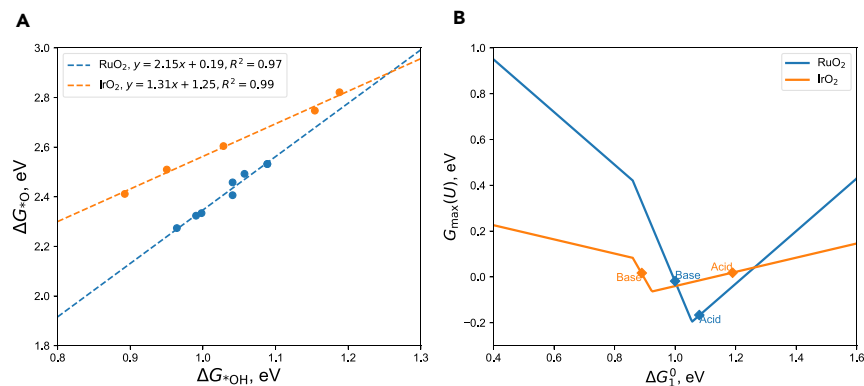


Figure 5. Results of applying the proposed methodology to the experimental data on RuO₂(110) and IrO₂(110)

(A) Scaling relations for RuO₂(110) and IrO₂(110) based on experimentally determined pH-dependent adsorption free energies of the *O and *OH intermediates.^{53,54}

(B) Generalized volcano plots based on the *O vs. *OH scaling relation for RuO₂(110) and IrO₂(110) at U = 1.60 V vs. RHE. The values for the data points of ΔG₁⁰ in acid (pH = 1) and base (pH = 12.9) are summarized in Table S1.

evident that RuO₂(110) is more active than IrO₂(110) for both acidic and alkaline conditions, which is consistent with the experimentally reported activity trends (cf. Table S2).

While Kuo and coworkers concluded in their pioneering work that the application of the Sabatier principle based on the adsorption free energies ΔG₁⁰ and ΔG₂⁰ does not allow comprehending the activity trends of IrO₂(110) and RuO₂(110),^{53,54} we emphasize that volcano plots with an explicit inclusion of the *O vs. *OH scaling relation intercept are able to reproduce their pH-dependent activity trends (cf. Table S2). This represents a major improvement over previously published simplified volcano models that rely only on the *OOH vs. *OH scaling relation.⁷⁴ In addition, our reported methodology also goes beyond the concept of overpotential-dependent volcano plots previously proposed by one of the authors, where activity trends for IrO₂(110) and RuO₂(110) at different pH values were not captured in the analysis.⁷⁵

DISCUSSION

While the discussion of the OER activity volcano plot has been governed by the *OOH vs. *OH scaling relation¹³ in the last decade, the OER volcano plot is invariant with respect to this scaling relation, as evident from recent works demonstrating that an alteration of the intercept ξ_2' deviating from the conventional value of 3.20 eV has basically no impact on the volcano shape or the preferred reaction mechanism.³⁹ A different situation though is encountered with the *O vs. *OH scaling relation, given that the present work highlights the significant effect of the intercept ξ_1' on the OER volcano plot. While the values $\gamma_1 = 0.60$ and $\xi_1' = 1.57$ eV from Divanis' work³⁷ refer to a dataset of transition-metal oxides, we emphasize that the corresponding values reported by Karmodak et al.⁸ for transition-metal dichalcogenides are $\gamma_1 = 0.46$ and $\xi_1' = 1.23$ eV. The clear difference between these datasets indicates that different classes of materials may follow a dissimilar *O vs. *OH scaling relation. It could even be the case that the *O vs. *OH scaling relation changes for different reaction mechanisms in the OER, which, if true, would enable the design of OER catalysts based on the preferred mechanistic pathways. The recent analysis of Man and Tranca indicates that the *O vs. *OH scaling relation is correlated to the electrocatalytic activity of metal oxides in the OER in that highly active OER catalysts reveal

a medium-sized value of the intercept $\xi'_1 = 1.81$ eV, whereas inactive OER catalysts are found for $\xi'_1 = 0.78$ eV or $\xi'_1 = 2.78$ eV.⁷⁰ Therefore, we propose that it may be beneficial to optimize materials in a homologous series by taking the *O vs. *OH scaling relation rather than the *OOH vs. *OH scaling relation as a reference.

We note that in previous works, it has already been discussed that the breaking of the *OOH vs. *OH scaling relation does not guarantee to obtain an electrocatalyst with higher intrinsic activity,^{63,68} and it may even cause optimization in the wrong direction toward lower activities. On the other hand, optimization (rather than breaking) of the *O vs. *OH scaling relation could potentially enable fine-tuning of electrocatalysts toward the OER. In this context, it is suggested that the *O vs. *OH scaling relation of transition-metal oxide-based RuO₂ and IrO₂ (cf. Figure 5A) may serve as a benchmark due to the high intrinsic activities of these materials for OER in acid. For other material classes, it might be purposeful to optimize their intercept ξ'_1 toward that of transition-metal oxide-based RuO₂ and IrO₂ as it can be assumed that such modification may be accompanied by an increased intrinsic activity. It is yet important to note the caveats of the above train of thought. Firstly, the energetics of the *O vs. *OH scaling relation is much more prone to scatter than that of the *OOH vs. *OH scaling relation. Hence, the determination of an intercept reveals higher uncertainty due to larger error bars. Secondly, the activity at the peak of the volcano depends very little on the scaling relation intercept. This renders the optimization of materials for the OER by the *O vs. *OH scaling relation more complex and error-prone than by using the conventional *OOH vs. *OH scaling relation.

Finally, we would like to provide a physical interpretation of why different intercepts for the *O vs. *OH scaling relation are not only observed among different material classes but even for different nanoparticle catalysts. It was demonstrated in previous works by Calle-Vallejo, Sautet, and coworkers that the intercept, ξ , of adsorbate-energy scaling relations is related to the geometric structure of adsorption sites.^{76,77} The classification of different adsorption sites is made possible by the concept of generalized coordination number, and different coordination numbers have been shown to reveal dissimilar intercepts in adsorbate-energy scaling relations.^{78,79} Further evidence was provided in a recent communication by Vogt,⁸⁰ outlining that σ - and π -bonded adsorbates on metal surfaces follow dissimilar intercepts. This finding is particularly relevant to the present case of the *O vs. *OH scaling relation as it is conventionally considered that the *O adsorbate may contain a π -bond, whereas the *OH intermediate consists of a σ -bond only. Therefore, we argue that a thorough investigation of the *O vs. *OH scaling relation intercept is urgently called for in future studies to further comprehend the factors that govern the OER activity on the atomic scale. These investigations may benefit from our advanced volcano plots including the sensitivity of the *O vs. *OH scaling relation to identify material motifs with high intrinsic OER activity for energy conversion.

Conclusions

Volcano plots have gained tremendous popularity as a tool to comprehend the activity trends of (electro-)catalytic processes including the OER by relying on the analysis of simple adsorption free energies. While the initial approach relied on a single mechanistic description and approximated the electrocatalytic activity by a single binding energy,^{13,41} recent advancements in the data-driven construction of volcano plots point out the necessity of applying advanced descriptors^{51,52} to determine the electrocatalytic activity as well as to factor various mechanistic pathways into the analysis.^{39,67} The evaluation of various mechanisms is enabled by the scaling relations between the *OH, *O, and *OOH intermediates in the OER.^{19–23} Here, it is

important to note that the considered scaling relation between the *O and OH adsorbates, both in the initial picture as well as in recent works,^{13,39,43,67} has relied so far on a simplification by neglecting the term ξ_1' (cf. Equation 12), which refers to the intercept of this scaling relation.

In the present work, we discuss the impact of the scaling relation intercept between the *O and *OH intermediates on the activity volcano plot of the OER, indicating that this intercept not only affects the location of the apex but also influences the preferred mechanism in the volcano plot (cf. Figure 3). Strikingly, it is possible to observe two minima in the volcano plot, one global and one local, depending on the intercept value of the *O vs. *OH scaling relation. This finding could serve as an additional explanation for the pressing issue in that no breakthrough in the OER^{5,81} has been achieved so far since optimization to the local minimum is difficult to achieve.

While we believe that new ways of thinking are needed to contribute to a breakthrough in the OER, we offer a new train of thought relating to catalyst discovery and optimization by referring to the *O vs. *OH scaling relation rather than the scaling relation between the *OOH and OH adsorbates. This procedure is benchmarked by the reproduction of experimental pH-dependent activity trends of IrO₂(110) and RuO₂(110) in the OER (cf. Figure 5). We believe that future works in this direction are required to shed further light on the significance of the O vs. *OH scaling relation to control the electrocatalytic activity of OER catalysts on the atomic scale.

EXPERIMENTAL PROCEDURES

Resource availability

Lead contact

Further information and requests for resources should be directed to and will be fulfilled by the lead contact, Kai S. Exner (kai.exner@uni-due.de).

Materials availability

No unique reagents were generated in this study.

Data and code availability

The code for the generalized volcano plot generation is available in the Zenodo repository⁵⁵ under <https://doi.org/10.5281/zenodo.11151309> and is publicly available as of the date of publication.

SUPPLEMENTAL INFORMATION

Supplemental information can be found online at <https://doi.org/10.1016/j.checat.2024.101039>.

ACKNOWLEDGMENTS

M.S. and K.S.E. acknowledge funding from the RESOLV Cluster of Excellence, funded by the Deutsche Forschungsgemeinschaft under Germany's Excellence Strategy – EXC 2033–390677874 – RESOLV. K.S.E. thanks the Ministry of Culture and Science of the Federal State of North Rhine-Westphalia (NRW Return Grant) and the CRC/TRR247: "Heterogeneous Oxidation Catalysis in the Liquid Phase" (project number 388390466-TRR 247) for financial support. This article is based upon the work from COST Action 18234, supported by COST (European Cooperation in Science and Technology).

AUTHOR CONTRIBUTIONS

M.S.: methodology, software, formal analysis, investigation, data curation, writing – original draft, writing – review & editing, and visualization. K.S.E.: conceptualization, resources, writing – original draft, writing – review & editing, supervision, project administration, and funding acquisition.

DECLARATION OF INTERESTS

The authors declare no competing interests.

Received: March 21, 2024

Revised: May 13, 2024

Accepted: June 4, 2024

Published: July 1, 2024

REFERENCES

1. Tripkovic, V., Hansen, H.A., and Vegge, T. (2017). From 3D to 2D Co and Ni Oxyhydroxide Catalysts: Elucidation of the Active Site and Influence of Doping on the Oxygen Evolution Activity. *ACS Catal.* **7**, 8558–8571. <https://doi.org/10.1021/acscatal.7b02712>.
2. Tripkovic, V., Hansen, H.A., Garcia-Lastra, J.M., and Vegge, T. (2018). Comparative DFT+U and HSE Study of the Oxygen Evolution Electrocatalysis on Perovskite Oxides. *J. Phys. Chem. C* **122**, 1135–1147. <https://doi.org/10.1021/acs.jpcc.7b07660>.
3. Fabbri, E., and Schmidt, T.J. (2018). Oxygen Evolution Reaction—The Enigma in Water Electrolysis. *ACS Catal.* **8**, 9765–9774. <https://doi.org/10.1021/acscatal.8b02712>.
4. Tripkovic, V., Hansen, H.A., and Vegge, T. (2018). Computational Screening of Doped α -MnO₂ Catalysts for the Oxygen Evolution Reaction. *ChemSusChem* **11**, 629–637. <https://doi.org/10.1002/cssc.201701659>.
5. Zeradjanin, A.R. (2018). Is a major breakthrough in the oxygen electrocatalysis possible? *Curr. Opin. Electrochem.* **9**, 214–223. <https://doi.org/10.1016/j.coelec.2018.04.006>.
6. Pan, F., Jin, T., Yang, W., Li, H., Cao, Y., Hu, J., Zhou, X., Liu, H., and Duan, X. (2021). Theory-guided design of atomic Fe–Ni dual sites in N,P-co-doped C for boosting oxygen evolution reaction. *Chem Catal.* **1**, 734–745. <https://doi.org/10.1016/j.checat.2021.06.017>.
7. Liu, S., Ji, Y., Yang, S., Li, L., Shao, Q., Hu, Z., Pao, C.-W., Chen, J.-L., Chan, T.-S., Zhu, T., et al. (2021). Spontaneous amorphous oxide-interfaced ultrafine noble metal nanoclusters for unexpected anodic electrocatalysis. *Chem Catal.* **1**, 1104–1117. <https://doi.org/10.1016/j.checat.2021.08.016>.
8. Karmodak, N., Bursi, L., and Andreussi, O. (2022). Oxygen Evolution and Reduction on Two-Dimensional Transition Metal Dichalcogenides. *J. Phys. Chem. Lett.* **13**, 58–65. <https://doi.org/10.1021/acs.jpcclett.1c03431>.
9. Barlocco, I., Cipriano, L.A., Di Liberto, G., and Pacchioni, G. (2023). Modeling Hydrogen and Oxygen Evolution Reactions on Single Atom Catalysts with Density Functional Theory: Role of the Functional. *Adv. Theory Simul.* **6**, 2200513. <https://doi.org/10.1002/adts.202200513>.
10. Wang, H., Liu, X., Liu, G., Wang, Y., Du, X., and Li, J. (2023). Copper doping-induced high-valence nickel-iron-based electrocatalyst toward enhanced and durable oxygen evolution reaction. *Chem Catal.* **3**, 100552. <https://doi.org/10.1016/j.checat.2023.100552>.
11. Zhang, Y., Zhang, L., Wang, J.-Q., and Kim, G. (2023). A-site-induced structural transformation to improve OER activity and stability in SOEC. *Chem Catal.* **3**, 100558. <https://doi.org/10.1016/j.checat.2023.100558>.
12. McCrory, C.C.L., Jung, S., Peters, J.C., and Jaramillo, T.F. (2013). Benchmarking Heterogeneous Electrocatalysts for the Oxygen Evolution Reaction. *J. Am. Chem. Soc.* **135**, 16977–16987. <https://doi.org/10.1021/ja407115p>.
13. Man, I.C., Su, H.Y., Calle-Vallejo, F., Hansen, H.A., Martínez, J.I., Inoglu, N.G., Kitchin, J., Jaramillo, T.F., Nørskov, J.K., and Rossmeisl, J. (2011). Universality in Oxygen Evolution Electrocatalysis on Oxide Surfaces. *ChemCatChem* **3**, 1159–1165. <https://doi.org/10.1002/cctc.201000397>.
14. Karmodak, N., and Andreussi, O. (2021). Oxygen Evolution on MoS₂ Edges: Activation through Surface Oxidation. *J. Phys. Chem. C* **125**, 10397–10405. <https://doi.org/10.1021/acs.jpcc.1c02210>.
15. Calle-Vallejo, F., Martínez, J.I., and Rossmeisl, J. (2011). Density functional studies of functionalized graphitic materials with late transition metals for oxygen reduction reactions. *Phys. Chem. Chem. Phys.* **13**, 15639–15643. <https://doi.org/10.1039/c1cp21228a>.
16. Calle-Vallejo, F., Martínez, J.I., García-Lastra, J.M., Abad, E., and Koper, M.T.M. (2013). Oxygen reduction and evolution at single-metal active sites: Comparison between functionalized graphitic materials and protoporphyrins. *Surf. Sci.* **607**, 47–53. <https://doi.org/10.1016/j.susc.2012.08.005>.
17. Svane, K.L., and Rossmeisl, J. (2022). Theoretical Optimization of Compositions of High-Entropy Oxides for the Oxygen Evolution Reaction. *Angew. Chem. Int. Ed.* **61**, e202201146. <https://doi.org/10.1002/anie.202201146>.
18. Nørskov, J.K., Rossmeisl, J., Logadottir, A., Lindqvist, L., Kitchin, J.R., Bligaard, T., and Jónsson, H. (2004). Origin of the overpotential for oxygen reduction at a fuel-cell cathode. *J. Phys. Chem. B* **108**, 17886–17892. <https://doi.org/10.1021/jp047349j>.
19. Bligaard, T., Nørskov, J.K., Dahl, S., Matthiesen, J., Christensen, C.H., and Sehested, J. (2004). The Brønsted–Evans–Polanyi relation and the volcano curve in heterogeneous catalysis. *J. Catal.* **224**, 206–217. <https://doi.org/10.1016/j.jcat.2004.02.034>.
20. Montemore, M.M., and Medlin, J.W. (2014). Scaling relations between adsorption energies for computational screening and design of catalysts. *Catal. Sci. Technol.* **4**, 3748–3761. <https://doi.org/10.1039/C4CY00335G>.
21. Medlin, J.W., and Montemore, M.M. (2015). Heterogeneous catalysis: Scaling the rough heights. *Nat. Chem.* **7**, 378–380. <https://doi.org/10.1038/nchem.2245>.
22. Greeley, J. (2016). Theoretical Heterogeneous Catalysis: Scaling Relationships and Computational Catalyst Design. *Annu. Rev. Chem. Biomol. Eng.* **7**, 605–635. <https://doi.org/10.1146/annurev-chembioeng-080615-034413>.
23. M, V., Singh, S., Bononi, F., Andreussi, O., and Karmodak, N. (2023). Thermodynamic and kinetic modeling of electrocatalytic reactions using a first-principles approach. *J. Chem. Phys.* **159**, 111001. <https://doi.org/10.1063/5.0165835>.
24. Koper, M.T.M. (2013). Theory of multiple proton–electron transfer reactions and its implications for electrocatalysis. *Chem. Sci.* **4**, 2710. <https://doi.org/10.1039/c3sc50205h>.
25. Koper, M.T. (2011). Thermodynamic theory of multi-electron transfer reactions: Implications for electrocatalysis. *J. Electroanal. Chem.* **660**, 254–260. <https://doi.org/10.1016/j.jelechem.2010.10.004>.
26. Exner, K.S. (2021). Why the optimum thermodynamic free-energy landscape of the

- oxygen evolution reaction reveals an asymmetric shape. *Mater. Today Energy* 21, 100831. <https://doi.org/10.1016/j.mtener.2021.100831>.
27. Razaq, S., and Exner, K.S. (2022). Statistical analysis of breaking scaling relation in the oxygen evolution reaction. *Electrochim. Acta* 412, 140125. <https://doi.org/10.1016/j.electacta.2022.140125>.
28. Ooka, H., Huang, J., and Exner, K.S. (2021). The Sabatier Principle in Electrocatalysis: Basics, Limitations, and Extensions. *Front. Energy Res.* 9, 654460. <https://doi.org/10.3389/fenrg.2021.654460>.
29. Quaino, P., Juarez, F., Santos, E., and Schmickler, W. (2014). Volcano plots in hydrogen electrocatalysis – uses and abuses. *Beilstein J. Nanotechnol.* 5, 846–854. <https://doi.org/10.3762/bjnano.5.96>.
30. Stratton, S.M., Zhang, S., and Montemore, M.M. (2023). Addressing complexity in catalyst design: From volcanos and scaling to more sophisticated design strategies. *Surf. Sci. Rep.* 78, 100597. <https://doi.org/10.1016/j.surfrep.2023.100597>.
31. Cepitis, R., Kongi, N., Rossmesl, J., and Ivaništšev, V. (2023). Surface Curvature Effect on Dual-Atom Site Oxygen Electrocatalysis. *ACS Energy Lett.* 8, 1330–1335. <https://doi.org/10.1021/acsenergylett.3c00068>.
32. Nwaokorie, C.F., and Montemore, M.M. (2022). Alloy Catalyst Design beyond the Volcano Plot by Breaking Scaling Relations. *J. Phys. Chem. C* 126, 3993–3999. <https://doi.org/10.1021/acs.jpcc.1c10484>.
33. Chen, J., Chen, Y., Li, P., Wen, Z., and Chen, S. (2018). Energetic Span as a Rate-Determining Term for Electrocatalytic Volcanos. *ACS Catal.* 8, 10590–10598. <https://doi.org/10.1021/acscatal.8b03008>.
34. Xiao, M., Chen, Y., Zhu, J., Zhang, H., Zhao, X., Gao, L., Wang, X., Zhao, J., Ge, J., Jiang, Z., et al. (2019). Climbing the Apex of the ORR Volcano Plot via Binuclear Site Construction: Electronic and Geometric Engineering. *J. Am. Chem. Soc.* 141, 17763–17770. <https://doi.org/10.1021/jacs.9b08362>.
35. Vijh, A. (1974). Volcano relationships in catalytic reactions on oxides. *J. Catal.* 33, 385–391. [https://doi.org/10.1016/0021-9517\(74\)90285-1](https://doi.org/10.1016/0021-9517(74)90285-1).
36. Barlocco, I., Di Liberto, G., and Pacchioni, G. (2024). New scaling relationships for the oxygen evolution reaction on single atom catalysts. *Catal. Today* 427, 114409. <https://doi.org/10.1016/j.cattod.2023.114409>.
37. Divanis, S., Kutlusoy, T., Ingmer Boye, I.M., Man, I.C., and Rossmesl, J. (2020). Oxygen evolution reaction: a perspective on a decade of atomic scale simulations. *Chem. Sci.* 11, 2943–2950. <https://doi.org/10.1039/C9SC05897D>.
38. Exner, K.S. (2023). How data-driven approaches advance the search for materials relevant to energy conversion and storage. *Mater. Today Energy* 36, 101364. <https://doi.org/10.1016/j.mtener.2023.101364>.
39. Exner, K.S. (2023). On the mechanistic complexity of oxygen evolution: potential-dependent switching of the mechanism at the volcano apex. *Mater. Horiz.* 10, 2086–2095. <https://doi.org/10.1039/D3MH00047H>.
40. Rossmesl, J., Logadottir, A., and Nørskov, J.K. (2005). Electrolysis of water on (oxidized) metal surfaces. *Chem. Phys.* 319, 178–184. <https://doi.org/10.1016/j.chemphys.2005.05.038>.
41. Rossmesl, J., Qu, Z.-W., Zhu, H., Kroes, G.-J., and Nørskov, J.K. (2007). Electrolysis of water on oxide surfaces. *J. Electroanal. Chem.* 607, 83–89. <https://doi.org/10.1016/j.jelechem.2006.11.008>.
42. Sargeant, E., Illas, F., Rodríguez, P., and Calle-Vallejo, F. (2021). Importance of the gas-phase error correction for O₂ when using DFT to model the oxygen reduction and evolution reactions. *J. Electroanal. Chem.* 896, 115178. <https://doi.org/10.1016/j.jelechem.2021.115178>.
43. Abild-Pedersen, F., Greeley, J., Studt, F., Rossmesl, J., Munter, T.R., Moses, P.G., Skúlason, E., Bligaard, T., and Nørskov, J.K. (2007). Scaling Properties of Adsorption Energies for Hydrogen-Containing Molecules on Transition-Metal Surfaces. *Phys. Rev. Lett.* 99, 016105. <https://doi.org/10.1103/PhysRevLett.99.016105>.
44. Calle-Vallejo, F., Martínez, J.I., García-Lastra, J.M., Rossmesl, J., and Koper, M.T.M. (2012). Physical and Chemical Nature of the Scaling Relations between Adsorption Energies of Atoms on Metal Surfaces. *Phys. Rev. Lett.* 108, 116103. <https://doi.org/10.1103/PhysRevLett.108.116103>.
45. Halck, N.B., Petrykin, V., Krtil, P., and Rossmesl, J. (2014). Beyond the volcano limitations in electrocatalysis – oxygen evolution reaction. *Phys. Chem. Chem. Phys.* 16, 13682–13688. <https://doi.org/10.1039/C4CP00571F>.
46. Nong, H.N., Falling, L.J., Bergmann, A., Klingenhof, M., Tran, H.P., Spöri, C., Mom, R., Timoshenko, J., Zichittella, G., Knop-Gericke, A., et al. (2020). Key role of chemistry versus bias in electrocatalytic oxygen evolution. *Nature* 587, 408–413. <https://doi.org/10.1038/s41586-020-2908-2>.
47. Fang, Y.-H., and Liu, Z.-P. (2010). Mechanism and Tafel Lines of Electro-Oxidation of Water to Oxygen on RuO₂ (110). *J. Am. Chem. Soc.* 132, 18214–18222. <https://doi.org/10.1021/ja1069272>.
48. Busch, M., Ahlberg, E., and Panas, I. (2011). Electrocatalytic oxygen evolution from water on a Mn(III–V) dimer model catalyst—A DFT perspective. *Phys. Chem. Chem. Phys.* 13, 15069–15076. <https://doi.org/10.1039/c0cp02132f>.
49. Busch, M. (2018). Water oxidation: From mechanisms to limitations. *Curr. Opin. Electrochem.* 9, 278–284. <https://doi.org/10.1016/j.coelec.2018.06.007>.
50. Binninger, T., and Doublet, M.-L. (2022). The Ir–OOO–Ir transition state and the mechanism of the oxygen evolution reaction on IrO₂ (110). *Energy Environ. Sci.* 15, 2519–2528. <https://doi.org/10.1039/D2EE00158F>.
51. Exner, K.S. (2020). A universal descriptor for the screening of electrode materials for multiple-electron processes: Beyond the thermodynamic overpotential. *ACS Catal.* 10, 12607–12617. <https://doi.org/10.1021/acscatal.0c03865>.
52. Razaq, S., and Exner, K.S. (2023). Materials Screening by the Descriptor $G_{\max}(\eta)$: The Free-Energy Span Model in Electrocatalysis. *ACS Catal.* 13, 1740–1758. <https://doi.org/10.1021/acscatal.2c03997>.
53. Kuo, D.-Y., Kawasaki, J.K., Nelson, J.N., Kloppenburg, J., Hautier, G., Shen, K.M., Schlom, D.G., and Suntivich, J. (2017). Influence of Surface Adsorption on the Oxygen Evolution Reaction on IrO₂ (110). *J. Am. Chem. Soc.* 139, 3473–3479. <https://doi.org/10.1021/jacs.6b11932>.
54. Kuo, D.-Y., Paik, H., Kloppenburg, J., Faeth, B., Shen, K.M., Schlom, D.G., Hautier, G., and Suntivich, J. (2018). Measurements of Oxygen Electrodesorption Energies and Oxygen Evolution Reaction on RuO₂ (110): A Discussion of the Sabatier Principle and Its Role in Electrocatalysis. *J. Am. Chem. Soc.* 140, 17597–17605. <https://doi.org/10.1021/jacs.8b09657>.
55. Sokolov, M., and Exner, K.S. (2024). Generalized Volcano Plots (Code) (Zenodo). <https://doi.org/10.5281/ZENODO.11151309>.
56. Exner, K.S. (2024). Toward data- and mechanistic-driven volcano plots in electrocatalysis. *Electrochem. Sci. Adv.* 4, e2200014. <https://doi.org/10.1002/elsa.202200014>.
57. Abild-Pedersen, F. (2016). Computational catalyst screening: Scaling, bond-order and catalysis. *Catal. Today* 272, 6–13. <https://doi.org/10.1016/j.cattod.2015.08.056>.
58. Busch, M., Halck, N.B., Kramm, U.I., Siahrostami, S., Krtil, P., and Rossmesl, J. (2016). Beyond the top of the volcano? – A unified approach to electrocatalytic oxygen reduction and oxygen evolution. *Nano Energy* 29, 126–135. <https://doi.org/10.1016/j.nanoen.2016.04.011>.
59. Murdachaew, G., and Laasonen, K. (2018). Oxygen Evolution Reaction on Nitrogen-Doped Defective Carbon Nanotubes and Graphene. *J. Phys. Chem. C* 122, 25882–25892. <https://doi.org/10.1021/acs.jpcc.8b08519>.
60. Wan, H., Østergaard, T.M., Arnarson, L., and Rossmesl, J. (2019). Climbing the 3D Volcano for the Oxygen Reduction Reaction Using Porphyrin Motifs. *ACS Sustainable Chem. Eng.* 7, 611–617. <https://doi.org/10.1021/acssuschemeng.8b04173>.
61. Sinha, S., Vegge, T., and Hansen, H.A. (2023). Bending the ORR Scaling Relations on Zirconium Oxynitride for Enhanced Oxygen Electrocatalysis. *ChemCatChem* 15, e202300349. <https://doi.org/10.1002/cctc.202300349>.
62. Kozuch, S., and Shaik, S. (2011). How to Conceptualize Catalytic Cycles? The Energetic Span Model. *Acc. Chem. Res.* 44, 101–110. <https://doi.org/10.1021/ar1000956>.
63. Exner, K.S. (2021). Why the breaking of the OOH versus OH scaling relation might cause decreased electrocatalytic activity. *Chem Catal.* 1, 258–271. <https://doi.org/10.1016/j.checat.2021.06.011>.
64. Exner, K.S. (2022). Beyond the thermodynamic volcano picture in the nitrogen reduction

- reaction over transition-metal oxides: Implications for materials screening. *Chin. J. Catal.* **43**, 2871–2880. [https://doi.org/10.1016/S1872-2067\(21\)64025-1](https://doi.org/10.1016/S1872-2067(21)64025-1).
65. Exner, K.S. (2023). On the concept of metal–hydrogen peroxide batteries: improvement over metal–air batteries? *Energy Adv.* **2**, 522–529. <https://doi.org/10.1039/D3YA00002H>.
66. Exner, K.S. (2023). Steering Selectivity in the Four-Electron and Two-Electron Oxygen Reduction Reactions: On the Importance of the Volcano Slope. *ACS Phys. Chem. Au* **3**, 190–198. <https://doi.org/10.1021/acspyschemau.2c00054>.
67. Exner, K.S. (2023). Importance of the Walden Inversion for the Activity Volcano Plot of Oxygen Evolution. *Adv. Sci.* **10**, 2305505. <https://doi.org/10.1002/adv.202305505>.
68. Govindarajan, N., García-Lastra, J.M., Meijer, E.J., and Calle-Vallejo, F. (2018). Does the breaking of adsorption-energy scaling relations guarantee enhanced electrocatalysis? *Curr. Opin. Electrochem.* **8**, 110–117. <https://doi.org/10.1016/j.coelec.2018.03.025>.
69. Over, H. (2021). Fundamental Studies of Planar Single-Crystalline Oxide Model Electrodes (RuO₂, IrO₂) for Acidic Water Splitting. *ACS Catal.* **11**, 8848–8871. <https://doi.org/10.1021/acscatal.1c01973>.
70. Man, I., and Tranca, I. (2024). Derived Trends of the Oxygen Adsorption Energy Using the Simplistic Model of the Thermodynamic Potential for Oxygen Evolution Reaction. Preprint. <https://doi.org/10.2139/ssrn.4821664>.
71. Exner, K.S. (2023). Importance of the volcano slope to comprehend activity and selectivity trends in electrocatalysis. *Curr. Opin. Electrochem.* **39**, 101284. <https://doi.org/10.1016/j.coelec.2023.101284>.
72. Groenenboom, M.C., Anderson, R.M., Horton, D.J., Basdogan, Y., Roeper, D.F., Policastro, S.A., and Keith, J.A. (2017). Doped Amorphous Ti Oxides To Deoptimize Oxygen Reduction Reaction Catalysis. *J. Phys. Chem. C* **121**, 16825–16830. <https://doi.org/10.1021/acs.jpcc.7b04210>.
73. Stoerzinger, K.A., Qiao, L., Biegalski, M.D., and Shao-Horn, Y. (2014). Orientation-Dependent Oxygen Evolution Activities of Rutile IrO₂ and RuO₂. *J. Phys. Chem. Lett.* **5**, 1636–1641. <https://doi.org/10.1021/jz500610u>.
74. Briquet, L.G.V., Sarwar, M., Mugo, J., Jones, G., and Calle-Vallejo, F. (2017). A New Type of Scaling Relations to Assess the Accuracy of Computational Predictions of Catalytic Activities Applied to the Oxygen Evolution Reaction. *ChemCatChem* **9**, 1261–1268. <https://doi.org/10.1002/cctc.201601662>.
75. Exner, K.S. (2020). Overpotential-Dependent Volcano Plots to Assess Activity Trends in the Competing Chlorine and Oxygen Evolution Reactions. *Chemelectrochem* **7**, 1448–1455. <https://doi.org/10.1002/celec.202000120>.
76. Kolb, M.J., Loffreda, D., Sautet, P., and Calle-Vallejo, F. (2021). Structure-sensitive scaling relations among carbon-containing species and their possible impact on CO₂ electroreduction. *J. Catal.* **395**, 136–142. <https://doi.org/10.1016/j.jcat.2020.12.026>.
77. Calle-Vallejo, F., Loffreda, D., Koper, M.T.M., and Sautet, P. (2015). Introducing structural sensitivity into adsorption–energy scaling relations by means of coordination numbers. *Nat. Chem.* **7**, 403–410. <https://doi.org/10.1038/nchem.2226>.
78. Brito-Ravicini, A., and Calle-Vallejo, F. (2022). Interplaying coordination and ligand effects to break or make adsorption-energy scaling relations. *Explorations* **2**, 20210062. <https://doi.org/10.1002/EXP.20210062>.
79. Calle-Vallejo, F. (2023). The ABC of Generalized Coordination Numbers and Their Use as a Descriptor in Electrocatalysis. *Adv. Sci.* **10**, 2207644. <https://doi.org/10.1002/adv.202207644>.
80. Vogt, C. (2023). Adsorbate Bond Number Dependency for σ - and π -bonds in Linear Scaling Relationships. *J. Phys. Chem. C* **127**, 5416–5424. <https://doi.org/10.1021/acs.jpcc.3c00727>.
81. Seh, Z.W., Kibsgaard, J., Dickens, C.F., Chorkendorff, I., Nørskov, J.K., and Jaramillo, T.F. (2017). Combining theory and experiment in electrocatalysis: Insights into materials design. *Science* **355**, eaad4998. <https://doi.org/10.1126/science.aad4998>.